

## Fall, classification, and exposure history of the Mifflin L5 chondrite

Noriko T. KITA<sup>1\*</sup>, Kees C. WELTEN<sup>2</sup>, John W. VALLEY<sup>1</sup>, Michael J. SPICUZZA<sup>1</sup>,  
Daisuke NAKASHIMA<sup>1</sup>, Travis J. TENNER<sup>1</sup>, Takayuki USHIKUBO<sup>1</sup>, Glenn J. MACPHERSON<sup>3</sup>,  
Linda WELZENBACH<sup>3</sup>, Philipp R. HECK<sup>4,5</sup>, Andrew M. DAVIS<sup>5,6</sup>, Matthias M. M. MEIER<sup>7,8</sup>,  
Rainer WIELER<sup>7</sup>, Marc W. CAFFEE<sup>9</sup>, Matthias LAUBENSTEIN<sup>10</sup>, and Kunihiko NISHIZUMI<sup>2</sup>

<sup>1</sup>Department of Geoscience, University of Wisconsin-Madison, Madison, Wisconsin 53706, USA

<sup>2</sup>Space Sciences Laboratory, University of California, Berkeley, California 94720, USA

<sup>3</sup>Department of Mineral Sciences, National Museum of Natural History, Smithsonian Institution, Washington,  
District of Columbia 20560, USA

<sup>4</sup>Robert A. Pritzker Center for Meteoritics and Polar Studies, Department of Geology, The Field Museum,  
1400 South Lake Shore Drive, Chicago, Illinois 60605, USA

<sup>5</sup>Chicago Center for Cosmochemistry, The University of Chicago, 5734 South Ellis Avenue, Chicago, Illinois 60637–1433, USA

<sup>6</sup>Department of the Geophysical Sciences and Enrico Fermi Institute, The University of Chicago, Chicago, Illinois 60637, USA

<sup>7</sup>Department of Earth Sciences, ETH Zürich, Zürich CH-8092, Switzerland

<sup>8</sup>Department of Geology, Lund University, Sölvegatan 12, Lund SE-22362, Sweden

<sup>9</sup>Department of Physics, Purdue University, West Lafayette, Indiana 47907, USA

<sup>10</sup>Laboratori Nazionali del Gran Sasso, I.N.F.N., S.S. 17/bis km 18 + 910, Assergi (AQ), I-67100, Italy

\*Corresponding author. E-mail: noriko@geology.wisc.edu

(Received 07 February 2012; revision accepted 04 January 2013)

---

**Abstract**—The Mifflin meteorite fell on the night of April 14, 2010, in southwestern Wisconsin. A bright fireball was observed throughout a wide area of the midwestern United States. The petrography, mineral compositions, and oxygen isotope ratios indicate that the meteorite is a L5 chondrite fragmental breccia with light/dark structure. The meteorite shows a low shock stage of S2, although some shock-melted veins are present. The U,Th-He age is 0.7 Ga, and the K-Ar age is 1.8 Ga, indicating that Mifflin might have been heated at the time of the 470 Ma L-chondrite parent body breakup and that U, Th-He, and K-Ar ages were partially reset. The cosmogenic radionuclide data indicate that Mifflin was exposed to cosmic rays while its radius was 30–65 cm. Assuming this exposure geometry, a cosmic-ray exposure age of  $25 \pm 3$  Ma is calculated from cosmogenic noble gas concentrations. The low  $^{22}\text{Ne}/^{21}\text{Ne}$  ratio may, however, indicate a two-stage exposure with a longer first-stage exposure at high shielding. Mifflin is unusual in having a low radiogenic gas content combined with a low shock stage and no evidence of late stage annealing; this inconsistency remains unexplained.

---

### INTRODUCTION

A bright fireball was seen by many observers in parts of Wisconsin, Iowa, and Illinois on the night of April 14, 2010. A camera on the roof of the Atmospheric and Oceanic Sciences Building at the University of Wisconsin-Madison (UW-Madison) captured two images of the fireball at 10:06 p.m. (3:06 UT) (Fig. 1). A National Oceanic and Atmospheric Administration (NOAA) Doppler radar recorded the track in southwestern Wisconsin across the Mifflin Township (Fries and Fries 2010), where residents heard

explosions at the same time. Numerous meteorites fell as a shower in a 20 km long strewn field centered on Mifflin Township (Fig. 2). When the fireball disintegrated at an altitude of approximately 28 km, it released energy equivalent to the detonation of approximately 20 tons of TNT. Data collected by scientists at the NASA Marshall Space Flight Center (Huntsville, Alabama), indicate that the meteoroid that produced this fireball was approximately 1 meter in diameter (Yeomans 2010). Within a few weeks, more than 70 stones totaling >3.5 kg, were collected. The meteorite was named “Mifflin” after the township that



Fig. 1. Photograph of the bright fireball observed over southwestern Wisconsin (April 14, 2010, 10:06 P.M., 3:06 UT) from the fall of the Mifflin meteorite. Two images were taken with 10 seconds interval that show the fireball. The image shown in this figure is the second one. Photo courtesy of Atmospheric and Oceanic Sciences and Space Science and Engineering Center, UW-Madison. Two bright lines are from airplane tracks.

includes the center of the strewn field and was classified as an L5 chondrite (Garvie 2012). In this article, we report the recovery, petrography, mineral chemistry,

oxygen isotopic ratios, noble gases, and cosmogenic nuclides of the Mifflin meteorite.

## RECOVERY

At the time of the meteorite fall, one resident of Mifflin Township heard a noise similar to hail falling on a metal rooftop. The first stone recovered had hit the metal roof of a shed and was found the following morning by this person. This specimen was brought to the Geology Museum at UW-Madison for identification (#1, 7.4 g, Fig. 3a). Within a week of the fall, several stones were displayed to the public at the UW-Madison Geology Museum and pictures of individual specimens (see Fig. S1) were posted on the Department of Geoscience website. Some of the pieces were later donated as a type specimen (#2, 21.1 g, Fig. 3b) and for chemical and isotopic analyses for classification (#6, 13.4 g, Fig. 3c). Many pieces had broken surfaces with light/dark-brecciated textures, which aided identification of the meteorites by individuals searching the strewn field. As shown in Fig. 2, stones fell in a 20 km long region centered in Mifflin Township, which overlaps with the Doppler radar track. More than 70 stones and fragments with a total mass of more than 3.5 kg were recovered in the area within a few weeks of the fall. The best estimate

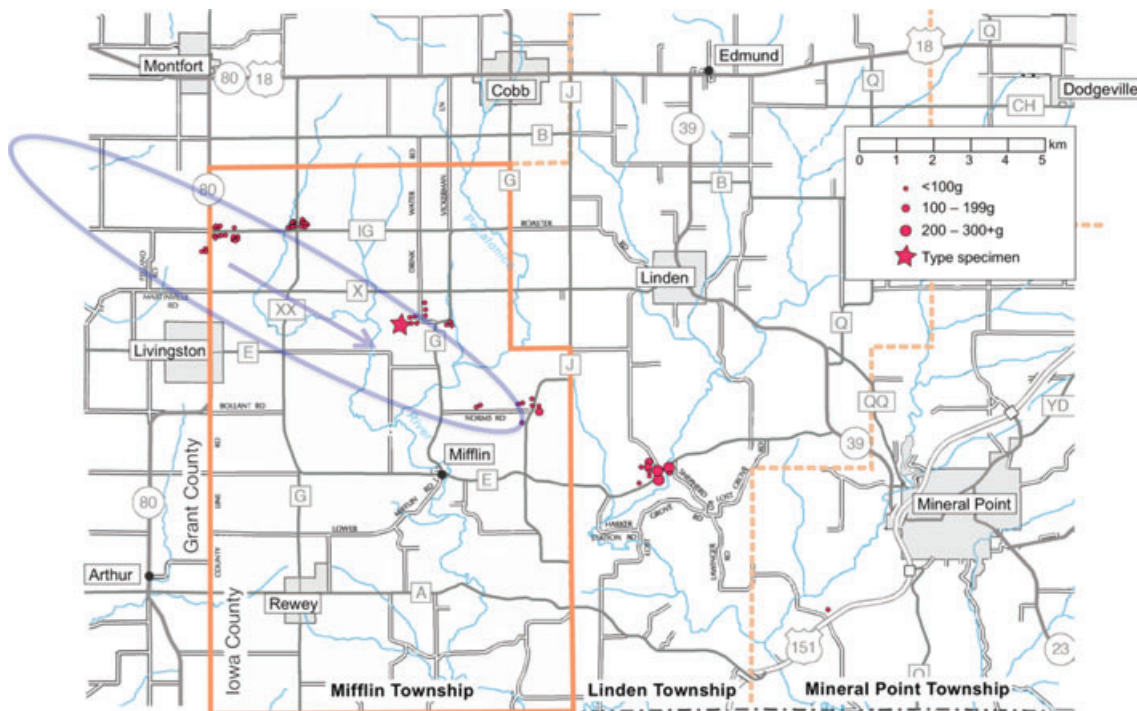


Fig. 2. Strewn field map of samples of the Mifflin meteorite. The meteorites fell mostly in Mifflin Township (outlined in orange). The blue ellipse indicates the location of the NOAA Doppler radar track. The direction of meteorite fall is shown as a blue arrow. Names of small towns and villages are shown in the rectangle boxes and their areas are shaded with gray. No meteorites were found within these towns and villages. The first stone that was recovered fell very close to the location of the type specimen. Information about locations of most stones courtesy of Atul Kumar.

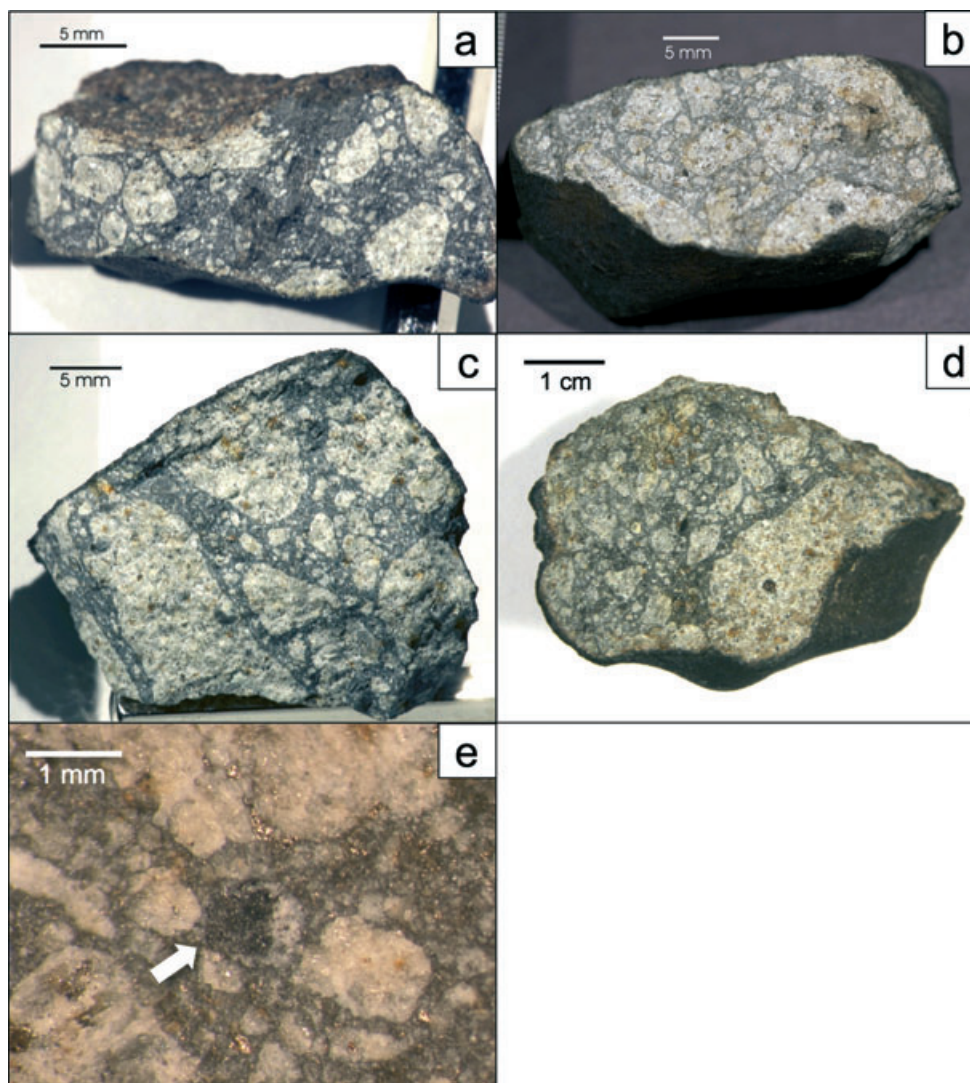


Fig. 3. Pictures of the Mifflin meteorite, recovered within a few days of the fall. a) The first stone (#1, 7.4 g) recovered the morning after the fall, b) fragment #2 (21 g), type specimen, c) fragment #6 (13.4 g), and d) Me 5109 (48 g). All of these samples show light clasts with dark matrix brecciated textures. Stone #1 is completely free of orange-colored stain on metal grains, in contrast to minor amounts of stain on other stones that were recovered after a few days and exposed to rain. e) Binocular microscope photo of a black clast from the broken surface of fragment #6. The black clast, indicated by the arrow, is located within dark matrix.

of the fall coordinates is  $42^{\circ}54'27''\text{N}$ ,  $90^{\circ}21'56''\text{W}$  (designated by a star in Fig. 2), the location where the type specimen was found. One specimen was found near highway US-151, which is the southeast end of the strewn field. The larger specimens ( $>200$  g) were found beyond the recorded Doppler radar track and toward the southeast end of the strewn field; the largest stone (332 g) was also found in this area. In contrast, most specimens found in the northwestern part of the strewn field are smaller than 100 g. These include a small fragment found by an elementary school student on the grounds of the Iowa-Grant Elementary School during a TV interview. One of the larger stones recovered in this area (Me 5109, 48 g, Fig. 3d), was donated to the Field Museum and

used for petrographic studies, as well as for cosmogenic radionuclide and noble gas analyses. The mass distribution of the recovered stones is consistent with the direction of atmospheric entry from the northwest to the southeast, as also indicated by the Doppler radar track.

## ANALYTICAL METHODS

### Electron Microscopy

Petrographic characterization and the major element compositions of several minerals were determined by scanning electron microscope (SEM) and electron microprobe (EMP) analyses. At the UW-Madison, a

Hitachi S-3400 SEM was used for obtaining backscattered electron (BSE) images and a Cameca SX-51 EMP was used for analysis of silicates, oxides, and phosphates. At the University of Chicago, a JEOL JSB-5800 LV SEM with an Oxford/Link ISIS-300 X-ray microanalysis system was used to obtain elemental maps. At the Smithsonian Institution, a JEOL JXA-8900R electron microprobe was used for analysis of metal, and a FEI Nova nanoSEM 600 field-emission-gun SEM was used for BSE imaging and energy-dispersive X-ray analysis of phases.

### X-Ray Diffraction

Brecciated meteorites often contain foreign materials incorporated into the host material during impact processes on their parent body surfaces (e.g., Bischoff et al. 2006). The Tsukuba meteorite (H5-6), for example, contains phyllosilicate-rich fine-grained black clasts similar to hydrated carbonaceous chondrites (Nakashima et al. 2003). Accordingly, X-ray diffraction patterns were obtained from small fragments of potential foreign materials taken from the broken surface of the Mifflin meteorite (#6), using a Rigaku Rapid II X-ray diffraction system with a 2-D image plate (Mo  $K\alpha$  radiation) at the Department of Geoscience, UW-Madison. The samples were mounted on glass fibers (5  $\mu\text{m}$  in diameter) and exposed to X-rays for about 15 min.

### Oxygen Isotope Analyses

Oxygen isotope analyses of bulk chips (approximately 3 mg) of the Mifflin meteorite were conducted in the Stable Isotope Laboratory at the UW-Madison (Spicuzza et al. 2007), using a laser fluorination extraction line and a Finnigan MAT 251 mass spectrometer. An international garnet standard UWG-2 ( $\delta^{18}\text{O} = 5.80\text{‰}$  VSMOW; Valley et al. 1995) was analyzed before and after the meteorite sample measurements. Long-term reproducibility of the UWG-2 standard by laser fluorination (1SD; standard deviation) is approximately 0.05‰, 0.03‰, and 0.015‰ for  $\delta^{18}\text{O}$ ,  $\delta^{17}\text{O}$ , and  $\Delta^{17}\text{O}$  ( $=\delta^{17}\text{O}-0.52 \times \delta^{18}\text{O}$ ), respectively.

### Radionuclide Analysis by Gamma-Ray Spectroscopy

The activities of  $^{26}\text{Al}$  (half-life =  $7.05 \times 10^5$  yr) and other short-lived cosmogenic radionuclides as well as long-lived natural radionuclides of a 44.3 g fragment (from Me 5109) of Mifflin were measured using nondestructive gamma-ray spectroscopy (Arpesella 1996) at the underground facility of the Laboratori Nazionali del Gran Sasso (LNGS) in Italy. Gamma-ray

measurements of radionuclides with half-lives of several days or longer were started on a Ge detector ten days after the meteorite fall. The counting efficiency of each radionuclide was calculated using a Monte Carlo code. This code is validated through measurements and analyses of samples of well-known radionuclide activities and geometries. The uncertainties in the counting efficiency are conservatively estimated at 10% ( $1\sigma$ ).

### Radionuclide Analysis by Accelerator Mass Spectrometry

An approximately 1.2 g split from specimen Me 5109 was used for analysis of cosmogenic  $^{10}\text{Be}$  (half-life =  $1.36 \times 10^6$  yr),  $^{26}\text{Al}$ , and  $^{36}\text{Cl}$  ( $3.01 \times 10^5$  yr) by accelerator mass spectrometry (AMS). The metal fraction (about 6 wt%) was separated and purified with 0.2 N HCl and concentrated HF. The purified metal fraction (41.6 mg) and the nonmagnetic (stone) fraction (120 mg) were dissolved in  $\text{HNO}_3$  or in  $\text{HF}/\text{HNO}_3$  in the presence of Be, Al, and Cl carriers. After dissolution, a small aliquot was taken for major element analysis by atomic absorption spectroscopy. Be, Al, and Cl were chemically separated and the  $^{10}\text{Be}/\text{Be}$ ,  $^{26}\text{Al}/\text{Al}$ , and  $^{36}\text{Cl}/\text{Cl}$  ratios were measured by AMS at Purdue University (Sharma et al. 2000). The measured ratios are corrected for blanks and normalized to AMS standards (Sharma et al. 1990; Nishiizumi 2004; Nishiizumi et al. 2007). The radionuclide concentrations are converted to activities in disintegrations per minute per kg ( $\text{dpm kg}^{-1}$ ).

### Noble Gas Analysis

The noble gas analyses were performed at ETH Zürich. An approximately 0.35 g piece of specimen Me 5109 was split into four subsamples with masses ranging from 64 to 96 mg; each subsample contained different relative fractions of the light and the dark lithology. Three of the subsamples have some fusion crust, while the fourth aliquot (#4) is free of fusion crust. The concentrations and isotopic compositions of the light noble gases were measured in the four subsamples, following procedures described in Wieler et al. (1989). The  $1\sigma$  uncertainty of concentrations for He, Ne, and Ar is  $\pm 2\%$  and that of isotopic ratios is 2% for He and  $<0.5\%$  for Ne and Ar (Heber et al. 2009).

## RESULTS AND DISCUSSION

### Petrography

Most stones are partly to fully coated with fusion crust. This is consistent with breakup during atmospheric entry as indicated by the bright fireball and loud explosions. The broken surfaces of the meteorite reveal a

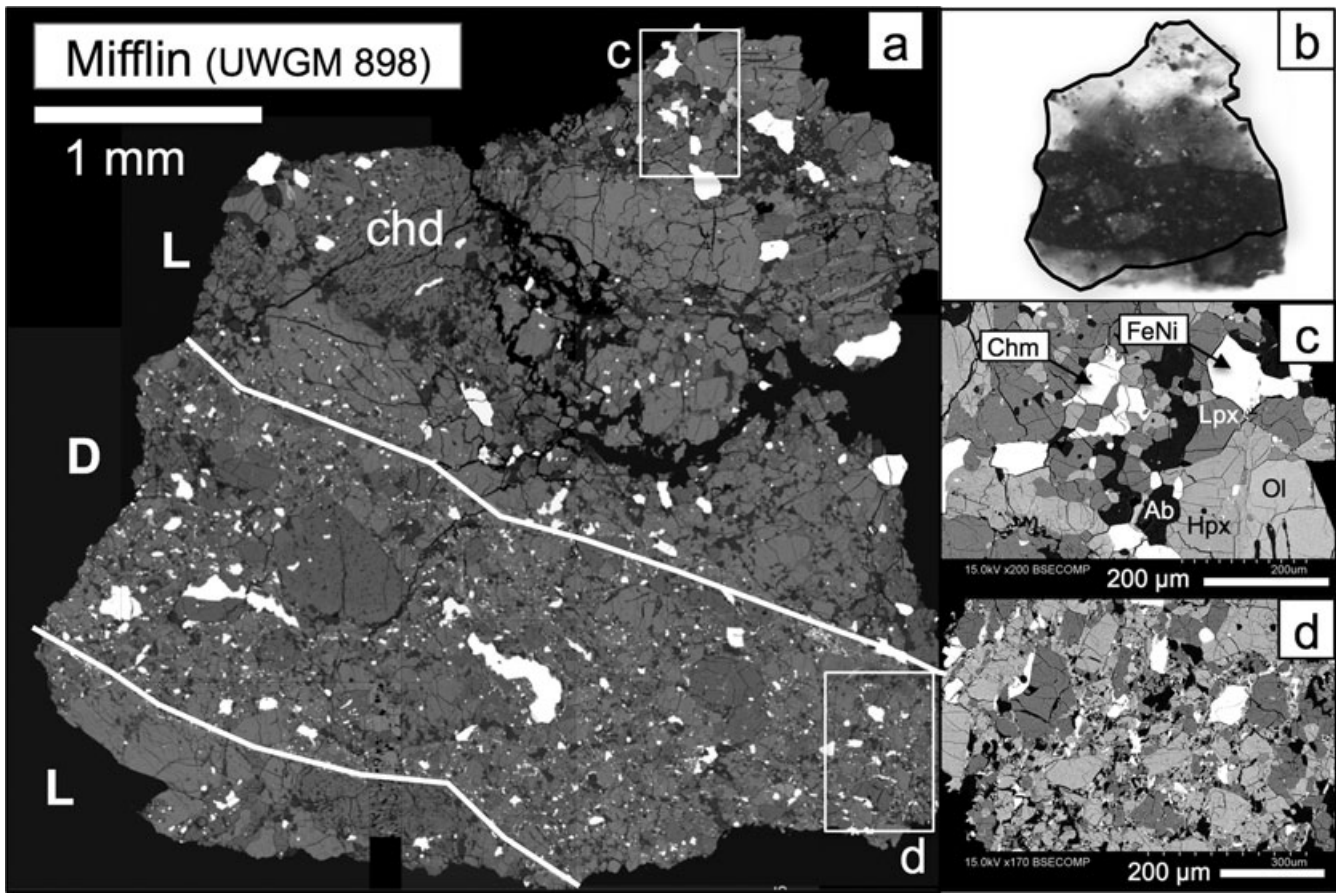


Fig. 4. a) BSE image of a polished section (UWGM 898) of Mifflin. Two white solid lines indicate the boundaries between dark matrix (D) and the light lithology (L). White frames (labeled as “c” and “d”) indicate areas shown in (c–d). b) Binocular microscope view of the same section, showing a band of dark matrix that contains small fragments of light clasts. The solid line indicates the outline of the polished surface. c) BSE image of light lithology, showing equilibrated textures and secondary minerals, including low-Ca pyroxene (Lpx), high-Ca pyroxene (Hpx), sodium-rich plagioclase (Pl), chromite (Chr), and Fe-Ni metal (FeNi). d) BSE image of dark matrix, consisting of sub-mm fragments of minerals that are rimmed with fine-grained metal-sulfide. Figures 4c and 4d are rotated 90 degrees relative to Fig. 4a.

brecciated texture with a dark matrix and light clasts (Fig. 3). The size of light clasts varies from smaller than 1 mm to more than 1 cm. Small fragments of light clasts are abundant in dark matrix areas. Although chondrules are not obvious in hand specimen, they are easily recognized in thin sections. Chondrule sizes typically are 0.5–1 mm. Binocular microscope examination of broken surfaces of the meteorite revealed the presence of sub-mm-size black clasts (Fig. 3e) that stand out against the dark matrix. The assigned shock stage is S2 because most of the larger olivine grains show undulose extinction, albeit weakly so (Stöffler et al. 1991).

The light/dark brecciated texture is apparent in hand specimens and in thin section with a petrographic microscope, but more difficult to recognize with electron microscope imaging. A BSE image in Fig. 4a is shown next to an incident-light photo (Fig. 4b) of the same area that illustrates a mm-wide band of dark matrix

separating light (unbrecciated) regions. Higher resolution BSE images of light (Fig. 4c) and dark regions (Fig. 4d) show their distinctive textures. The light regions are unbrecciated chondrite, in which the matrix is heavily recrystallized to a dense polygonal-granular texture dominated by 10–30 µm grains of olivine, pyroxene, and feldspar. Accessory phases include FeNi metal, troilite, chromite, and phosphates (merrillite and apatite). Chondrules (Fig. 4a) are up to approximately 1 mm in diameter. The boundary between chondrules and matrix is blurred. Nonetheless, the chondrules retain much of their original structure; porphyritic, barred, and radial varieties are recognizable (e.g., Figs. 5a and 5b). Glass is replaced by clear birefringent feldspar. Most low calcium pyroxene is orthorhombic, but sparse clinoenstatite (polysynthetic twinning) is preserved. Both kamacite and taenite (possibly also tetrataenite) are present, in some cases together in an exsolution relationship (Figs. 5c and

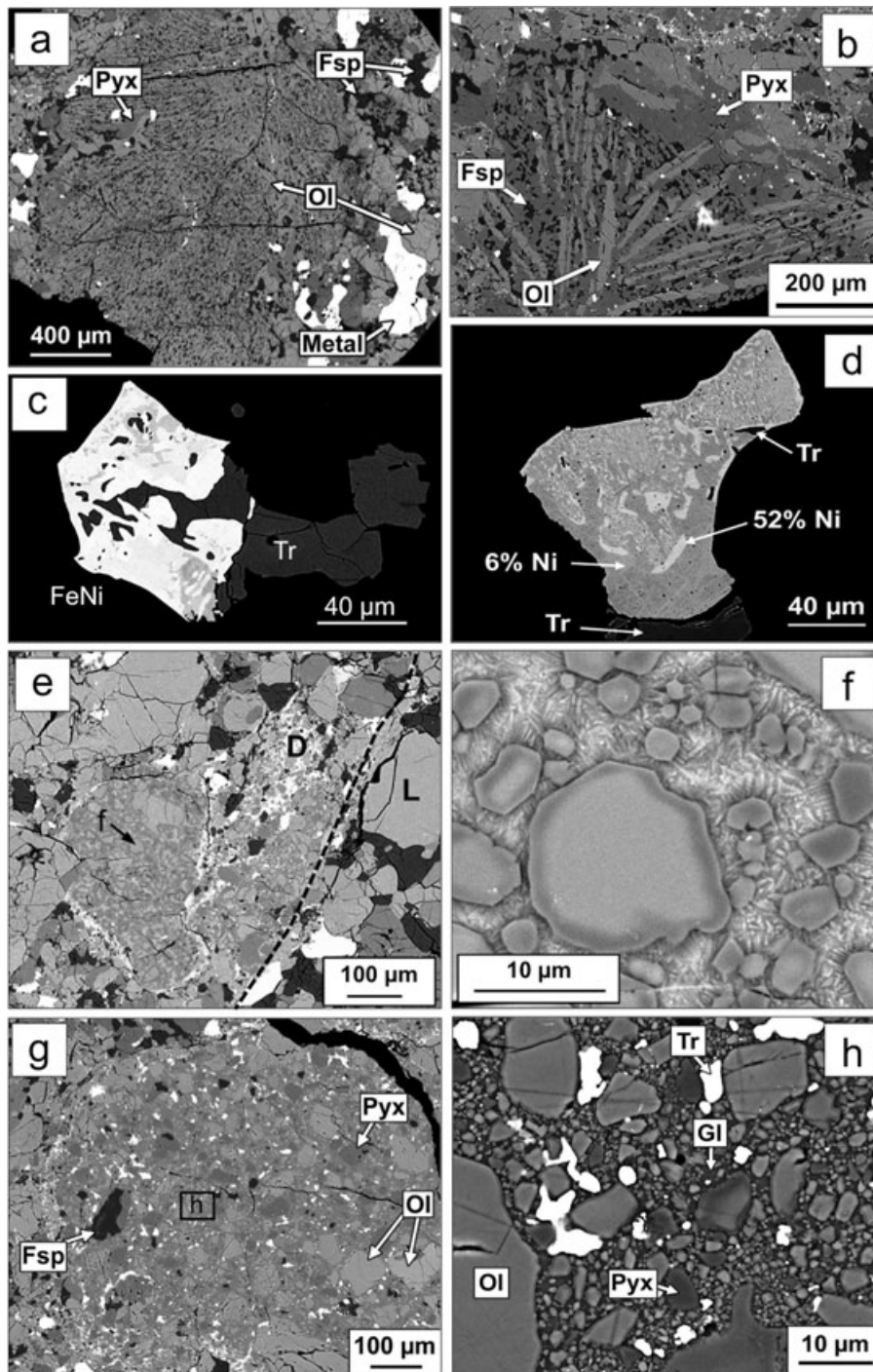


Fig. 5. Detailed BSE images of structures within Mifflin. a) Radial pyroxene chondrule. b) Barred olivine chondrule. c–d) Complex Ni zoning in metal particles. e) A sub-mm-sized melt clast located in dark matrix (D) near a light clast (L). The melt clast is coated by fine-grained metal and sulfide. The boundary of the two lithologies is shown as a dashed line. The arrow pointing to the center of the clast (labeled as “f”) indicates the area shown in (f). f) Expanded image of a melt clast containing zoned olivine grains. Dark zones correspond to Mg-rich olivine (approximately  $Fa_{16}$ ) and the brighter core of the large olivine grain is homogeneous at  $Fa_{25}$ . The mesostasis of the melt clast contains sub- $\mu$ m dendritic microcrystalites possibly with pyroxene composition. g) A large mm-sized melt clast containing multiple mineral fragments including olivine (Ol), pyroxene (Pyx), and plagioclase (Fsp). The rectangular box (labeled as “h”) indicates expanded view in (h). h) Mineral fragments including olivine, pyroxene, and sulfide (Tr) are set in glassy matrix (Gl).

5d) and elsewhere as simple composite grains. The dark (brecciated) portion of the chondrite consists of 30–100  $\mu\text{m}$ -sized mineral, lithic (light chondrite), and chondrule fragments all having sharp boundaries against one another and against the finely comminuted ( $\leq 10 \mu\text{m}$ ) interstitial material. Pyroxene again is mostly orthorhombic. Although feldspar is easily recognizable in the brecciated zones using BSE imaging, the dark nature and fine grain size of the matrix make it nearly impossible to see the feldspar with an optical microscope.

Distinctive melt regions up to several 100  $\mu\text{m}$  across are also present, within the dark lithology (Fig. 5e). The shapes of the melt regions themselves range from rounded to angular, implying that these are not in situ melt pockets but, rather, lithic clasts within the dark lithology. Some melt clasts consist of oscillatory zoned olivine grains, having rounded iron-rich cores overgrown by strongly zoned rims, enclosed within a microlite-rich glassy mesostasis (Fig. 5f). The rounded shapes of the olivine cores suggest that they experienced a moderate degree of partial melting followed by rapid cooling. Yet the preservation of olivine zonation in the melt clasts indicates that the clasts did not experience postshock annealing since incorporation into the Mifflin breccia. Other melt clasts (Figs. 5g and 5h) contain angular diverse mineral fragments with thin overgrowths, densely crowded within a small amount of glass, and indicating much smaller degrees of melting than the olivine-phyric clasts described above. These melt clasts are commonly surrounded by fine-grained metal- and sulfide-rich rims.

We extracted one of the “dark clasts” seen via binocular examination of meteorite surfaces, noted above, and split it into three fragments. They were examined by X-ray diffraction to determine if the clast might be a hydrated carbonaceous chondritic clast like those observed in some other ordinary chondrites (e.g., the Tsukuba H5-6 chondrite regolith breccias; Nakashima et al. 2003). However, the diffraction patterns indicate the presence of plagioclase and chromite, but no hydrated silicates. One of the fragments was mounted in epoxy, polished, and examined via SEM. The BSE image (Fig. 6a) and EDS spectra show it to consist of albite-rich plagioclase enclosing 1–10- $\mu\text{m}$ -sized euhedral chromite crystals, confirming the X-ray diffraction results. The plagioclase in this clast is distinctly more calcium-rich (approximately  $\text{An}_{23}$ ) than the interstitial plagioclase throughout the rest of the meteorite. The plagioclase-chromite assemblage resembles those reported in some ordinary chondrites that experienced shock heating (e.g., Xie et al. 2001; Rubin 2002), indicating that the intergrowths themselves may be the result of shock-induced melting. However, in this case the angular shapes of the black clasts suggest that such melting did not take place in situ but,

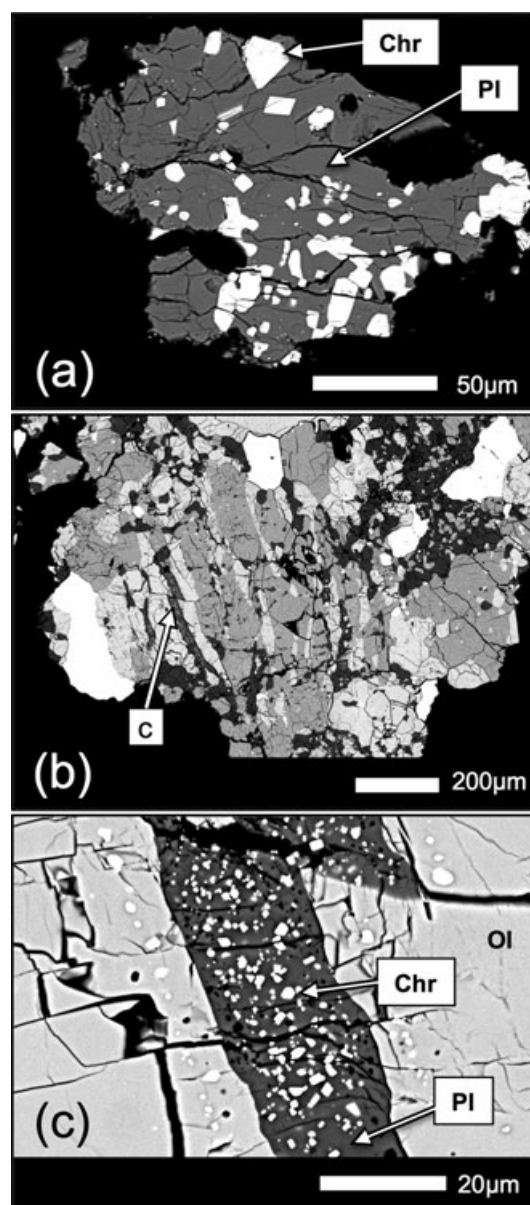


Fig. 6. BSE images of plagioclase-chromite regions in Mifflin. a) A fragment extracted from the black clast shown in Fig. 3e consists of chromite grains (Chr), 1–20  $\mu\text{m}$  in size, enclosed in plagioclase (Pl; approximately  $\text{An}_{23}$ ). b) A porphyritic chondrule within the light lithology (Fig. 4a) that has curious vein-like structures; the arrow indicates the rectangular area shown enlarged in (c), which reveals the vein to be filled with porous feldspathic glass (note tiny round bubbles) and minute chromite crystals; the glass has recrystallized to birefringent plagioclase, but the bubbles (black) are preserved.

rather, predated assembly of the Mifflin breccia. Similar plagioclase-chromite intergrowths are also observed in some areas within the light lithology (Figs. 6b and 6c). These plagioclase-bearing assemblages are different in texture from that of the normal interstitial plagioclase observed elsewhere in Mifflin (Fig. 4c).

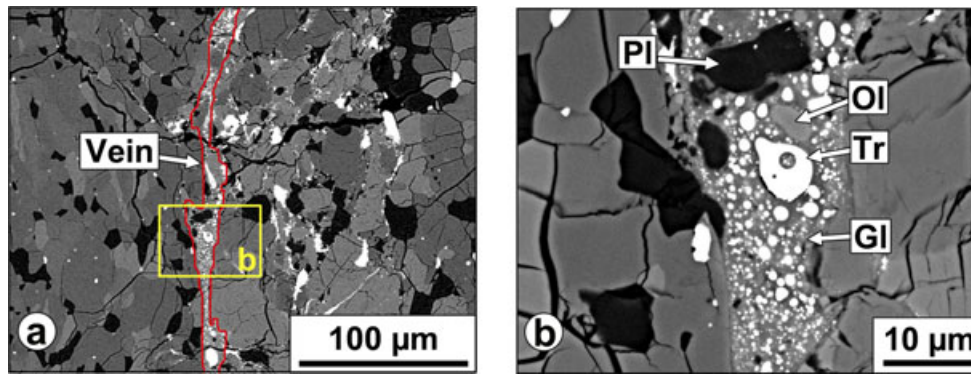


Fig. 7. BSE images of a shock-melt vein cross-cutting Mifflin. The image at left (a) shows an outline (red line) of the vein; the yellow box gives the location of the high magnification image shown in (b). The close-up in (b) shows rounded globules of troilite (Tr), plus partially resorbed relicts of plagioclase (Pl) and olivine (Ol), enclosed in glass (Gl).

Different from and independent of the melt clasts, the (possibly melted) chromite-plagioclase clasts are thin (up to approximately 20  $\mu\text{m}$ ) shock-melted veins that cross-cut the meteorite. Figure 7 shows one such vein; the globular nature of the sulfide sitting in homogeneous glass, plus the rounded (resorbed) shapes of the silicates, leave little doubt that melting on a very local scale has occurred in situ. Bischoff et al. (1983) showed that, even under relatively weak shock pressures consistent with a shock stage of S2, grain boundary melting may occur in porous fine-grained objects.

### Mineral Chemistry

Electron microprobe analyses of the major phases are given in Table 1.

We observed no detectable differences in the silicate compositions between the light and dark lithologies. Olivine, low-Ca pyroxene, and high-Ca pyroxene have average compositions of  $\text{Fa}_{25.4}$ ,  $\text{En}_{76.9}\text{Wo}_{1.4}\text{Fs}_{21.7}$ , and  $\text{En}_{46.8}\text{Wo}_{45.2}\text{Fs}_{8.0}$ , respectively, and, as shown in Table 1, exhibit very little compositional variation. These data are consistent with data reported for this meteorite earlier ( $\text{Fa}_{24.9} \pm 0.2$  and  $\text{Fs}_{21.1} \pm 0.2$ ; Garvie 2012). Such compositions are within the range found in L-chondrites (e.g., Brearley and Jones 1998) (see Fig. 8). Plagioclase has an average composition of  $\text{Ab}_{83.4}\text{An}_{10.9}\text{Or}_{5.8}$ . Both merrillite and chlorapatite are present, and their major and minor element compositions are consistent with those in equilibrated ordinary chondrites (Brearley and Jones 1998). As for the nonsilicates, we observed no detectable differences in major element compositions of phosphate and chromite from the light clast versus dark matrix areas. Major and minor element compositions of chromite are consistent with those observed in L-chondrites (Brearley and Jones 1998). Electron microprobe analyses of metal show 5.5 wt% Ni in kamacite and 50 wt% Ni in taenite. The Ni contents in

kamacite are in the range observed among L-chondrites (Brearley and Jones 1998).

The melt clasts and plagioclase-chromite areas have somewhat different mineral chemistry. The olivine crystals are clearly zoned (Fig. 5a) and have a compositional range of at least  $\text{Fa}_{16-26}$  (Table 1; column 2). Note also that the most Mg-rich compositions of these melt clast olivines are distinctly more forsteritic than those in the main light and dark lithologies. However, the MnO/FeO ratios of olivine in the melt clast (approximately 0.02) are indistinguishable from those in olivine grains in the rest of the meteorite, permissive of the possibility that the melt clast formed by partial melting of the main Mifflin lithology (albeit not necessarily in situ). EDS data (not given in the table) for plagioclase in the melt clasts and in the chromite-plagioclase regions indicate that it is more calcium-rich (approximately  $\text{An}_{23}$ ) than that in the light and dark lithologies.

### Oxygen Isotope Ratios

Four aliquots were analyzed for oxygen three isotopes, two each from the light clasts and dark matrix. The four analyses are indistinguishable within analytical error and show average values of  $\delta^{18}\text{O} = 4.84\text{‰}$ ,  $\delta^{17}\text{O} = 3.65\text{‰}$ , and  $\Delta^{17}\text{O} = 1.13\text{‰}$  VSMOW (Table 2). As shown in Fig. 9, the results from Mifflin are within the range observed for types 4–6 L-chondrites (Clayton et al. 1991). The lack of differences in oxygen isotope ratios from different lithologies indicates that dark matrix is made of brecciated fragments of the same materials in the light clasts. This is consistent with the indistinguishable major element compositions in mineral phases between both lithologies.

### Cosmogenic Radionuclides

The concentrations of cosmogenic radionuclides reflect the irradiation (shielding) conditions of a sample

Table 1. Major element compositions (wt.%) of minerals in Mifflin meteorite.

	Olivine		Pyroxene		Plagioclase
	Light, dark	Melt clast	Low-Ca	High-Ca	Light, dark
SiO <sub>2</sub>	37.86	38.67	56.53	55.09	64.97
TiO <sub>2</sub>	n.d. <sup>a</sup>	n.d.	0.19	0.46	0.04
Al <sub>2</sub> O <sub>3</sub>	n.d.	n.d.	0.19	0.54	21.19
Cr <sub>2</sub> O <sub>3</sub>	n.d.	0.18	0.10	0.79	n.d.
FeO	23.15	20.91	14.15	4.92	0.41
MgO	38.13	39.60	28.11	16.13	n.d.
MnO	0.48	0.43	0.47	0.24	n.d.
CaO	n.d.	n.d.	0.72	21.64	2.22
Na <sub>2</sub> O	n.d.	n.d.	n.d.	0.56	9.52
K <sub>2</sub> O	n.d.	n.d.	n.d.	n.d.	1.00
Total	99.62	99.79	100.47	100.38	99.35
N <sup>b</sup>	18	10	25	21	19
Avg. comp	Fa <sub>25.4</sub>	Fa <sub>22.9</sub>	En <sub>76.9</sub> Wo <sub>1.4</sub> Fs <sub>21.7</sub>	En <sub>46.8</sub> Wo <sub>45.2</sub> Fs <sub>8.0</sub>	An <sub>10.9</sub> Ab <sub>83.4</sub> Or <sub>5.8</sub>
Range	Fa <sub>24.7–25.9</sub>	Fa <sub>16–26</sub>	En <sub>75.9–77.6</sub> Wo <sub>1.0–1.9</sub> Fs <sub>20.8–22.6</sub>	En <sub>46.3–47.7</sub> Wo <sub>43.9–46.3</sub> Fs <sub>7.0–8.7</sub>	An <sub>10.2–13.1</sub> Ab <sub>80.8–85.0</sub> Or <sub>4.1–8.6</sub>

	Apatite	Merrillite	Chromite	Taenite	Kamacite		
FeO	0.31	0.50	TiO <sub>2</sub>	3.03	Fe	48.6	93.4
MgO	n.d.	3.42	Al <sub>2</sub> O <sub>3</sub>	6.04	Ni	50.3	5.5
CaO	52.68	46.29	Cr <sub>2</sub> O <sub>3</sub>	55.12			
Na <sub>2</sub> O	0.34	2.72	V <sub>2</sub> O <sub>3</sub>	0.69			
P <sub>2</sub> O <sub>5</sub>	40.79	45.88	FeO	30.48			
Cl	4.62	n.d.	MgO	2.57			
F	0.50	n.d.	MnO	0.67			
			ZnO	0.31			
Total	99.24	98.81		98.91		98.9	98.9
N <sup>b</sup>	15	18		31			

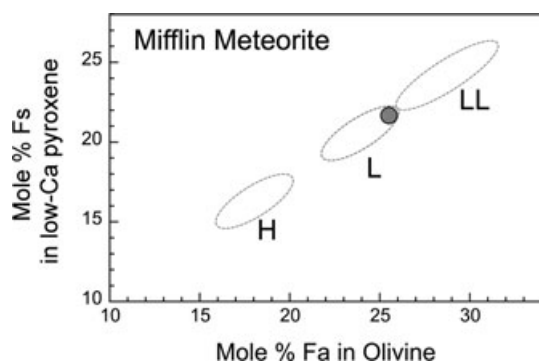
<sup>a</sup>n.d. = not detected.<sup>b</sup>Number of analyses.

Fig. 8. Mineral compositions of olivine and low-Ca pyroxene in Mifflin meteorite (excluding some data from melt clasts with Mg-rich olivine grains). The filled symbol shows the average compositions of Mifflin meteorite listed in Table 1. The ranges of H, L, and LL chondrite data are from Brearley and Jones (1998).

Table 2. Oxygen isotope ratios in Mifflin meteorite<sup>a</sup>.

Sample	Weight (mg)	$\delta^{18}\text{O}\text{‰}$ VSMOW	$\delta^{17}\text{O}\text{‰}$ VSMOW	$\Delta^{17}\text{O}\text{‰}$
Light clast, coarse	2.98	4.79	3.63	1.14
Light clast, fines	2.99	4.96	3.73	1.15
Dark matrix, fines	2.67	4.78	3.57	1.09
Dark matrix, gray	2.97	4.74	3.60	1.13
Average		4.84	3.65	1.13

<sup>a</sup>Long-term reproducibilities (1SD) of UWG-2 garnet standard are 0.05‰, 0.025‰, and 0.015‰ for  $\delta^{18}\text{O}$ ,  $\delta^{17}\text{O}$ , and  $\Delta^{17}\text{O}$ , respectively.

during the last few half-lives of cosmic-ray exposure (CRE), while the concentrations and isotopic ratios of cosmogenic noble gases provide information on the total irradiation time and average shielding conditions. We will show that the cosmogenic radionuclide data of Mifflin can

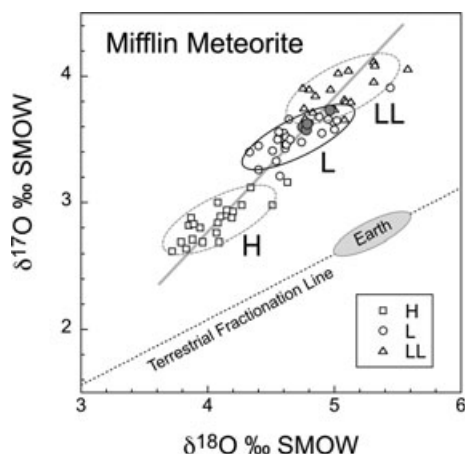


Fig. 9. Oxygen three-isotope ratios of Mifflin meteorites. Ordinary chondrite data are from Clayton et al. (1991). Mifflin meteorite data (filled symbols) plot within the range of bulk L-chondrites. Terrestrial fractionation line is shown as a dotted line. A solid gray line is the equilibrated chondrite line (ECL) of Clayton et al. (1991).

Table 3. Activities of cosmogenic radionuclides<sup>a</sup> (in dpm kg<sup>-1</sup>) in the Mifflin meteorite (Me 5109) measured by nondestructive gamma-ray spectroscopy.

Nuclide	Half-life	Mifflin	Torino <sup>b</sup>	OC range <sup>c</sup>
<sup>52</sup> Mn	5.6 days	26 ± 9	20 ± 2	9–26
<sup>48</sup> V	16.0 days	18 ± 2	21 ± 2	5–41
<sup>51</sup> Cr	27.7 days	63 ± 10	76 ± 7	28–130
<sup>7</sup> Be	53.1 days	98 ± 11	59 ± 6	30–210
<sup>58</sup> Co	70.9 days	12 ± 1	11 ± 1	1–26
<sup>56</sup> Co	77.3 days	8 ± 1	7.8 ± 0.8	3–120
<sup>46</sup> Sc	83.8 days	10 ± 1	10 ± 2	2–13
<sup>57</sup> Co	271.8 days	16 ± 2	16 ± 1	3–17
<sup>54</sup> Mn	312.3 days	117 ± 12	121 ± 2	28–160
<sup>22</sup> Na	2.60 yr	109 ± 11	80 ± 11	40–260
<sup>60</sup> Co	5.27 yr	11 ± 1	2.8 ± 0.3	0–220
<sup>26</sup> Al	7.05 × 10 <sup>5</sup> yr	50 ± 5	54 ± 1	36–100

<sup>a</sup>Activities are corrected to the time of fall and quoted errors with combined standard uncertainties.

<sup>b</sup>Torino H-chondrite (fell in May 1988; Bhandari et al. 1989).

<sup>c</sup>The observed range in ordinary chondrites (Evans et al. 1982; Bhandari et al. 2002).

be explained by a one-stage irradiation in a medium-sized meteoroid, while the noble gas data favor irradiation in a larger object. Activities of cosmogenic radionuclides in Mifflin, corrected to the time of fall, are given in Table 3 along with those of the Torino meteorite (Bhandari et al. 1989) as well as the observed activity ranges of ordinary chondrites for comparison (Evans et al. 1982; Bhandari et al. 2002). The U, Th, and K concentrations derived from the natural activities of <sup>235</sup>U, <sup>232</sup>Th, and <sup>40</sup>K in the Mifflin sample are 12 ± 1 ppb U, 46 ± 4 ppb Th, and

760 ± 80 ppm K, respectively. These values are consistent with the average L-chondrite concentrations (Wasson and Kallemeyn 1988; Kallemeyn et al. 1989). The <sup>22</sup>Na/<sup>26</sup>Al activity ratio of Mifflin is 2.2 ± 0.3, which is at the high end of the typical range of 1–2 observed for chondrite falls (e.g., Evans et al. 1982; Bhandari et al. 2002). Due to the similar production mechanism of <sup>22</sup>Na and <sup>26</sup>Al, the activity ratio of these two nuclides is insensitive to shielding conditions of the meteoroid. However, due to the short half-life of <sup>22</sup>Na (2.60 yr), the ratio is sensitive to short-term variations in the galactic cosmic-ray (GCR) flux, which in turn is modulated by the 11-year solar cycle. The relatively high <sup>22</sup>Na/<sup>26</sup>Al activity ratio observed in Mifflin is consistent with several years of low solar activity immediately before the fall; the low solar activity results in a higher GCR flux and thus a higher <sup>22</sup>Na concentration. The effects of the low solar activity were also observed in the Jesenice L6 chondrite that fell in April 2009 (Bischoff et al. 2011), while they are less pronounced in chondritic fragments of the Almahata Sitta meteorites, which fell in October 2008 (Bischoff et al. 2010). The short-lived radionuclides in Jesenice indicate it experienced nearly the same GCR flux and thus the same solar activity conditions as those seen by the Mifflin meteorite. Note that the short-lived radionuclides with half-lives of less than a year in Mifflin are also very similar to those observed in the Torino meteorite (Table 3), which fell in May, 1988, exactly two solar cycles (22 yr) prior to the Mifflin fall (Bhandari et al. 1989). This indicates that Mifflin and Torino experienced very similar GCR fluxes in the last year of their CRE, as would be expected on the basis of their fall times during periods of low solar activity.

The concentrations of <sup>10</sup>Be, <sup>26</sup>Al, and <sup>36</sup>Cl in metal and stone fractions are given in Table 4 along with several major element concentrations of these fractions. The measured concentrations of Ni and Co in the metal fraction are consistent with L-chondrite compositions. We made small corrections for <sup>10</sup>Be (1.2%) and <sup>26</sup>Al (5.5%) due to silicate contamination in the metal fraction by using the measured Mg concentration in the metal fraction. The <sup>10</sup>Be and <sup>26</sup>Al concentrations in the bulk sample are calculated to be 20.5 ± 0.6 and 61.5 ± 1.6 dpm kg<sup>-1</sup> based on the mass balance of stone and metal fractions, which are 94 and 6 wt%, respectively. The quoted uncertainties in Table 4 include uncertainties in the AMS measurements, but not the uncertainties in the absolute values of the AMS standards, which range from 1 to 3%.

#### Preatmospheric Size

Cosmogenic <sup>60</sup>Co is predominantly produced by thermal neutron capture on <sup>59</sup>Co, a reaction pathway that is very sensitive to meteoroid size and sample depth (Spergel et al. 1986). The measured <sup>60</sup>Co activity in Mifflin is 11 ± 1 dpm kg<sup>-1</sup>, indicating either irradiation

Table 4. Concentrations of major elements and cosmogenic radionuclides in the metal<sup>a</sup> and stone fractions of the Mifflin meteorite (Me 5109).

Fractions	Major elements (mg g <sup>-1</sup> ) <sup>b</sup>							Cosmogenic radionuclides (dpm kg <sup>-1</sup> ) <sup>c</sup>		
	Mg	Al	Ca	Mn	Fe	Co	Ni	<sup>10</sup> Be	<sup>26</sup> Al	<sup>36</sup> Cl
Metal	0.6	–	–	–	857	6.9	137	4.74 ± 0.10	3.63 ± 0.18	22.1 ± 0.7
Stone	169	12.5	13.6	2.6	173	–	5	21.7 ± 0.5	65 ± 2	8.0 ± 0.2

<sup>a</sup>Cosmogenic radionuclides in metal fraction are corrected for 0.4 wt% stone contamination (see text).

<sup>b</sup>Data obtained from atomic absorption spectroscopy.

<sup>c</sup>Data obtained from AMS.

Table 5. Concentrations (in 10<sup>-8</sup> cm<sup>3</sup> STP g<sup>-1</sup>) and isotopic ratios of noble gases in the Mifflin meteorite (Me 5109).

Sample	Weights (mg)	Lithology	<sup>3</sup> He	<sup>4</sup> He	$\frac{^{20}\text{Ne}}{^{22}\text{Ne}}$	<sup>21</sup> Ne	$\frac{^{22}\text{Ne}}{^{21}\text{Ne}}$	<sup>38</sup> Ar	<sup>40</sup> Ar	$\frac{^{36}\text{Ar}}{^{38}\text{Ar}}$	<sup>38</sup> Ar <sub>c</sub> <sup>a</sup>
#1	88.5	Light + Dark	22.9	357	0.838	6.81	1.051	1.10	1128	1.78	0.83
#2	91.2	Dark	19.5	312	0.848	6.46	1.056	1.06	1067	1.81	0.79
#3	63.9	Light	17.7	253	0.846	6.44	1.048	1.06	1139	1.62	0.84
#4	96.4	Dark	28.2	374	0.827	7.20	1.048	1.05	1045	1.51	0.85

<sup>a</sup>Concentrations of cosmogenic <sup>38</sup>Ar, which were calculated assuming that the measured <sup>36</sup>Ar/<sup>38</sup>Ar ratios are the mixtures of cosmogenic and trapped components with <sup>36</sup>Ar/<sup>38</sup>Ar ratios of 0.65, and 5.32, respectively.

in the near-center of an object with a preatmospheric radius ( $R$ ) of approximately 25 cm, or irradiation closer to the surface of an object with  $R > 30$  cm. The <sup>36</sup>Cl activity of  $22.1 \pm 0.7$  dpm kg<sup>-1</sup> in the metal fraction is consistent with  $R < 50$  cm (Leya and Masarik 2009). At this shielding condition, spallation reactions (mainly on Fe and Ca) produce a <sup>36</sup>Cl activity of  $6.5 \pm 0.5$  dpm kg<sup>-1</sup> in the stone fraction. On the other hand, the observed <sup>36</sup>Cl activity of  $8.0 \pm 0.2$  dpm kg<sup>-1</sup> in the stone fraction of Mifflin suggests that some of the <sup>36</sup>Cl ( $1.5 \pm 0.5$  dpm kg<sup>-1</sup>) was produced by thermal neutron capture, <sup>35</sup>Cl( $n,\gamma$ )<sup>36</sup>Cl. According to model calculations, the production rate ratio of neutron-capture <sup>60</sup>Co and <sup>36</sup>Cl, <sup>60</sup>Co/<sup>36</sup>Cl, is  $7 \pm 1$  in L-chondrites assuming 150 ppm of Cl and 600 ppm Co (Spergel et al. 1986). The observed neutron-capture <sup>36</sup>Cl activity of  $1.5 \pm 0.5$  dpm kg<sup>-1</sup> in the stone fraction of Mifflin is in good agreement with the predicted value of  $1.6 \pm 0.3$  dpm kg<sup>-1</sup>, based on neutron-capture <sup>60</sup>Co. This implies that the irradiation conditions of Mifflin were unchanged in the last approximately 1 Ma and that the Cl concentration (which was not measured) is close to the assumed value of 150 ppm.

The <sup>10</sup>Be concentrations in the bulk and metal fraction of Mifflin are  $20.5 \pm 0.6$  and  $4.74 \pm 0.10$  dpm kg<sup>-1</sup>, respectively, while those of <sup>26</sup>Al are  $61.5 \pm 1.6$  and  $3.63 \pm 0.20$  dpm kg<sup>-1</sup>, respectively. The <sup>26</sup>Al activity measured by AMS is significantly higher than that measured by gamma-ray spectroscopy. In the following discussion, we will adopt the weighted average of  $60.4 \pm 1.4$  dpm kg<sup>-1</sup> for <sup>26</sup>Al. The measured <sup>10</sup>Be and

<sup>26</sup>Al activities are consistent with predicted production rates at a position within 10 cm from the surface of a meteoroid with  $R = 30$ –65 cm (Leya and Masarik 2009).

The <sup>36</sup>Cl/<sup>10</sup>Be ratio of  $4.66 \pm 0.18$  in the metal fraction is in good agreement with the <sup>36</sup>Cl/<sup>10</sup>Be-<sup>10</sup>Be correlation that was obtained from a large set of meteorites with long exposure ages (Lavielle et al. 1999). The <sup>26</sup>Al/<sup>10</sup>Be ratio of  $0.77 \pm 0.04$  in the metal fraction also matches the average saturation ratio of  $0.71 \pm 0.05$  that was found in a large set of meteorites (e.g., Lavielle et al. 1999), as does the <sup>26</sup>Al/<sup>10</sup>Be ratio of  $3.0 \pm 0.1$  in bulk Mifflin. We thus conclude that the <sup>36</sup>Cl, <sup>26</sup>Al, and <sup>10</sup>Be activities in Mifflin were all produced by a single exposure to cosmic rays. All the cosmogenic radionuclide data from a single specimen (Me 5109) of the Mifflin meteorite are consistent with a cosmic-ray exposure near the surface of a meteoroid with a radius of 30–65 cm for at least several million years (longer than the mean-life of <sup>10</sup>Be). Fireball observations indicate a radius of approximately 50 cm, consistent with our conclusions.

### Noble Gases

The concentrations and isotopic ratios of the noble gases in four subsamples of Mifflin are given in Table 5. The <sup>3</sup>He concentration in the fusion-crust free sample (#4) is somewhat higher than in the other samples, indicating loss of He during atmospheric ablation for samples containing fusion crust. Sample #4 also has a 5–10% higher <sup>21</sup>Ne concentration than the three other samples, indicating that some Ne was also lost during atmospheric

ablation. In contrast, the concentrations of  $^{38}\text{Ar}$  are indistinguishable among the four samples (Table 5).

The measured  $^{20}\text{Ne}/^{22}\text{Ne}$  ratios (0.83–0.85) indicate that the Ne composition in Mifflin is purely cosmogenic with no solar-wind-derived contribution. This suggests Mifflin is not a regolith breccia, but a fragmental breccia. Gas-rich regolith breccias are very rare among L-chondrites (Bischoff et al. 2006), while fragmental breccias are quite common (Rubin et al. 1983). The measured  $^{22}\text{Ne}/^{21}\text{Ne}$  ratios in the four Mifflin samples are virtually identical, indicating that minor Ne losses during atmospheric entry did not affect the isotopic composition. The four samples yield an average ratio of  $1.051 \pm 0.004$  ( $1\sigma$ ). This value is at the low end of the range of 1.05–1.25 observed in ordinary chondrites (e.g., Masarik et al. 2001). The  $^3\text{He}/^{21}\text{Ne}$  ratios range from 2.75 to 3.92, but the ratios in three of the four samples are affected by loss of cosmogenic He from fusion crust. The ratio of 3.92 in sample #4 is also at the low end of the range in ordinary chondrites, but still falls on the  $^3\text{He}/^{21}\text{Ne}$  versus  $^{22}\text{Ne}/^{21}\text{Ne}$  correlation line observed in ordinary chondrites (e.g., Masarik et al. 2001). This indicates that this Mifflin sample did not suffer significant diffusive loss of cosmogenic He. These low  $^{22}\text{Ne}/^{21}\text{Ne}$  and  $^3\text{He}/^{21}\text{Ne}$  ratios suggest irradiation in a meteoroid with a radius of  $>40$  cm (Leya and Masarik 2009).

The measured  $^{36}\text{Ar}/^{38}\text{Ar}$  ratios in Mifflin range between 1.5–1.8, relative to the expected ratio of approximately 0.65 for the cosmogenic component. The elevated  $^{36}\text{Ar}/^{38}\text{Ar}$  ratio is probably due to a small trapped Ar component with a  $^{36}\text{Ar}/^{38}\text{Ar}$  ratio of 5.32, although it is also possible that Mifflin contains a sizeable amount of  $^{36}\text{Ar}_{\text{nc}}$  from the decay of neutron-capture-produced  $^{36}\text{Cl}$  (Bogard et al. 1995). If we assume that the  $^{36}\text{Ar}$  and  $^{38}\text{Ar}$  in Mifflin is a mixture of trapped and cosmogenic Ar, we can calculate the two endmember concentrations; the results for the cosmogenic  $^{38}\text{Ar}$  ( $^{38}\text{Ar}_c$ ) concentrations are shown in Table 5. The concentration of trapped  $^{36}\text{Ar}$  calculated by this method ( $1.0\text{--}1.4 \times 10^{-8}$   $\text{cm}^3$  STP  $\text{g}^{-1}$ ) is within the range of planetary Ar found in chondrites of petrologic types 5–6 (Marti 1967).

### Gas-Retention Age

Helium-4 has three possible sources: radiogenic, cosmogenic, and solar. There are no solar-wind-implanted noble gases so the radiogenic  $^4\text{He}$  in Mifflin is the residual after subtracting the cosmogenic component from the total. We assumed a cosmogenic  $^4\text{He}/^3\text{He}$  ratio of 6 (e.g., Alexeev 1998; Honda et al. 2002; Welten et al. 2003), which is consistent with the low  $^{22}\text{Ne}/^{21}\text{Ne}$  ratio (Leya and Masarik 2009). The average radiogenic  $^4\text{He}$  concentration in three of the four samples is  $207 \pm 13 \times 10^{-8}$   $\text{cm}^3$  STP  $\text{g}^{-1}$ ; in sample #3, the sample with the largest  $^3\text{He}$  loss (and probably the largest amount

of fusion crust), the concentration is approximately 30% lower. Using the U and Th concentrations obtained by gamma-ray spectroscopy, we obtain a U,Th-He age of  $0.71 \pm 0.07$  Ga. Using the measured  $^{40}\text{Ar}$  concentration in the fusion-crust free sample (#4) and the K concentration measured by gamma-ray spectroscopy, we obtain a K-Ar age of  $1.86 \pm 0.10$  Ga. Mifflin thus belongs to the large group of L-chondrites having short gas-retention ages (Heymann 1967). The discrepancy between the two gas-retention ages suggests that Mifflin may have experienced incomplete degassing of  $^{40}\text{Ar}$  and  $^4\text{He}$  during an event younger than 0.71 Ga. The most likely scenario involves loss of approximately 86% of radiogenic  $^{40}\text{Ar}$  and approximately 96% of radiogenic  $^4\text{He}$  during the catastrophic breakup event of the L-chondrite parent body at 470 Ma (e.g., Bogard 1995; Korochantseva et al. 2007). As discussed below, however, reconciling this implied catastrophic event with the low shock stage is problematic.

### Cosmic-Ray Exposure History

Since all cosmogenic radionuclide concentrations in specimen (Me 5109) are consistent with a simple irradiation near the surface of a meteoroid with a radius of 30–65 cm, we will first assume that Mifflin was exposed to cosmic rays in this geometry after its ejection from the parent body. The production rates of cosmogenic  $^3\text{He}$ ,  $^{21}\text{Ne}$ , and  $^{38}\text{Ar}$  in chondrites are generally calculated as a function of the cosmogenic  $^{22}\text{Ne}/^{21}\text{Ne}$  ratio. However, this technique is only applicable to samples with  $^{22}\text{Ne}/^{21}\text{Ne}$  ratios  $>1.08$  (e.g., Graf et al. 1990), and is not valid for Mifflin due to its low  $^{22}\text{Ne}/^{21}\text{Ne}$  ratio of approximately 1.05.

We calculate the CRE age based on the  $^{10}\text{Be}/^{21}\text{Ne}$  and  $^{26}\text{Al}/^{21}\text{Ne}$  ratios using the semiempirical model of Graf et al. (1990), assuming a simple (one stage) exposure history, in which the  $^{10}\text{Be}$  and  $^{26}\text{Al}$  concentrations serve as monitors for the shielding condition. Based on average production rate ratios of  $\text{P}(^{10}\text{Be})/\text{P}(^{21}\text{Ne}) = 0.141$  (Graf et al. 1990) and  $\text{P}(^{26}\text{Al})/\text{P}(^{21}\text{Ne}) = 0.41$  atom/atom (Welten et al. 2003), the measured  $^{10}\text{Be}/^{21}\text{Ne}$  and  $^{26}\text{Al}/^{21}\text{Ne}$  ratios of sample #4 yield CRE ages of 25.0 Ma for both methods. The same method using the model of Leya and Masarik (2009) yields CRE ages of 23.1 and 28.2 Ma, respectively. Assuming an uncertainty of 10–15% in the production rate ratios, we adopt an average CRE age of  $25 \pm 3$  Ma. This age is well outside the major peak at approximately 40 Ma in the CRE age histogram of L-chondrites, but falls close to the peak at approximately 28 Ma observed for L-chondrites with low radiogenic gas concentrations (Marti and Graf 1992). Note that L-chondrites with low concentration of

radiogenic gases are generally more shocked than other L-chondrites (Dodd and Jarosewich 1979; Stöffler et al. 1991), while the shock stage of Mifflin is very low (S2), thus Mifflin may not be a typical member of the 28 Ma peak.

The calculated CRE age is based on the assumption that Mifflin experienced a simple, one-stage exposure history. While the radionuclide data are consistent with a shallow irradiation depth, the cosmogenic noble gases may indicate a different exposure geometry. In particular, the low  $^{22}\text{Ne}/^{21}\text{Ne}$  ratio of 1.05 and the  $^3\text{He}/^{21}\text{Ne}$  ratio of 3.92 indicate a larger shielding depth. According to model calculations, these ratios are only obtained at depths of 30–50 cm within an object with radius >40 cm (Masarik et al. 2001). For this geometry, roughly 80–150 dpm kg<sup>-1</sup> of  $^{60}\text{Co}$  and 10–20 dpm kg<sup>-1</sup> of  $^{36}\text{Cl}$  (assuming 150 ppm of Cl) would be produced by thermal neutron capture alone. Production rates this high are inconsistent with the observed activities of both radionuclides. A possible explanation of this apparent discrepancy is a two-stage cosmic-ray irradiation. A first-stage exposure would have been in an object with a minimum radius of 60 cm, followed by a second-stage exposure in an object with a radius of 30–65 cm. Since all cosmogenic radionuclide concentrations are consistent with the latter irradiation geometry, the second-stage exposure was at least 2–3 Ma. Alternatively, the overwhelming fraction of the cosmogenic noble gases could have been produced in the first-stage exposure at a depth of 30–50 cm, thereby explaining the low  $^{22}\text{Ne}/^{21}\text{Ne}$  and  $^3\text{He}/^{21}\text{Ne}$  ratios. In this scenario, some of the  $^{36}\text{Ar}$  in Mifflin could also have been produced during this first-stage irradiation through decay of neutron-capture  $^{36}\text{Cl}$ . Based on neutron-capture  $^{36}\text{Cl}$  production rates of 10–20 dpm kg<sup>-1</sup> for the first-stage irradiation, we estimate that  $(0.5\text{--}1.0) \times 10^{-8} \text{ cm}^3 \text{ STP g}^{-1}$  of  $^{36}\text{Ar}$  could have been produced through decay of neutron-capture  $^{36}\text{Cl}$ . This would imply that nearly the entire inventory of measured  $^{36}\text{Ar}$  and  $^{38}\text{Ar}$  was produced by cosmic-ray exposure, and therefore the actual concentration of  $^{38}\text{Ar}_c$  would be up to 20% higher than the value reported in Table 5. We cannot determine the first-stage exposure age precisely since the shielding conditions of the first stage are not well constrained. The best estimate is 30–40 Ma, based on predicted  $^{21}\text{Ne}$  and  $^{38}\text{Ar}$  production rates (Graf et al. 1990). Although the two-stage exposure model is capable of explaining the cosmogenic nuclide results of the Mifflin meteorite, the complex irradiation conditions of the meteorite are not yet well constrained. Based on the above discussion, it is unlikely that Mifflin belongs to the 28 Ma exposure age peak. Although the ejection time of Mifflin from its parent body cannot be precisely determined, we conclude that Mifflin is most likely a fragment of a secondary L-chondrite parent body that

was formed during the collisional disruption of the main L-chondrite parent body at 470 Ma.

### Radiogenic Gas Loss and Formation of Breccia

Mifflin is the currently only known L-chondrite with low shock stage (S2) that shows dramatic losses of radiogenic  $^4\text{He}$  and  $^{40}\text{Ar}$  (nearly 90%). These radiogenic gas losses are generally associated with shock pressures of >35 GPa equivalent to shock stage S5 and S6 (Stöffler et al. 1991). Large radiogenic gas losses in meteorites with shock stage S1–S2 have been observed in several H-chondrites, but unlike Mifflin, they are associated with low  $^3\text{He}/^{21}\text{Ne}$  ratios and are attributed to solar heating in space as a meter-sized object (Schultz and Stöffler 1993). Abundant shock-induced melt can be one explanation for radiogenic gas losses. For example, a wide range of radiogenic gas losses among the moderately shocked ordinary chondrites (S3–S4) may be in part due to the variations in the abundance of shocked-melt (Stöffler et al. 1991). Similarly, the major breakup event of the L-chondrite parent body at approximately 470 Ma (e.g., Bogard 1995) resulted in highly shocked mineralogy (e.g., deformation of mineral structure, formation of high-pressure minerals, and shock melt) in many L-chondrites. However, other than the thin shock-melted veins such as that illustrated in Fig. 7, much of the evidence for shock-melting in Mifflin is in the form of melt clasts (Figs. 5–6) that pre-date assembly of the Mifflin breccia. Moreover, such clasts do not appear to represent a large mass fraction of Mifflin. Rubin (2002) suggested that postshock annealing could erase evidence for intense shock, but the preservation of undulose extinction in olivine and the clearly identifiable melt clasts and shock-melted veins are inconsistent with such an interpretation. Thus, the available evidence does not support the interpretation that localized melt formation is responsible for radiogenic He and Ar losses in Mifflin. One plausible scenario might be the increase in postshock temperatures under low shock pressures by mixing of hot shock melt with cool unshocked objects, as illustrated by Stöffler et al. (1991) who suggested multiple  $P$ – $T$  paths during a large impact crater formation. In this case, Mifflin could be the distal product of a large event that mixed impact melt debris with less-shocked material into a complex breccia, making it different from solar-wind gas-rich regolith breccias. More detailed work will be required to resolve this conundrum.

### CONCLUSIONS

Olivine and low-Ca pyroxene compositions and the oxygen isotope ratios of the Mifflin meteorite are consistent with it being a L-chondrite. The distinct chondrule margins and sizes of secondary minerals

( $\leq 50 \mu\text{m}$ ) indicate that the Mifflin meteorite is a type 5 chondrite. Mifflin has a brecciated light-dark structure, but the absence of solar-wind-implanted noble gases in both the light and the dark lithologies indicates that it is a fragmental breccia and not a regolith breccia. Mifflin presents a puzzle because, although the shock stage of the meteorite is S2 based on the undulose extinction of most of the large olivine grains, the content of radiogenic gases is unusually low. The latter is usually interpreted as the result of intense in situ shock-induced heating. However, although Mifflin does contain various types of partially melted objects that might be due to impact-induced heating processes, most of these (other than very thin shock-melted veins) appear to be clasts that predate assembly of the Mifflin breccia. Gas-retention ages of Mifflin are  $0.71 \pm 0.07 \text{ Ga}$  and  $1.86 \pm 0.10 \text{ Ga}$  for  $\text{U,Th-}^4\text{He}$  and  $^{40}\text{K-}^{40}\text{Ar}$  respectively. The discrepancy between the two gas-retention ages suggests that Mifflin may have experienced incomplete degassing of  $^{40}\text{Ar}$  and  $^4\text{He}$  during an event younger than 0.71 Ga. Reconciling this gas loss with the overall very low shock stage of Mifflin remains an unsolved conundrum.

Cosmogenic radionuclide data from Mifflin indicate that the meteorite was exposed to cosmic rays near the surface of an object with a radius of 30–65 cm for at least several million years. The CRE age of Mifflin is calculated to be  $25 \pm 3 \text{ Ma}$  using this exposure condition and noble gas concentrations. This CRE age may overlap with a peak in the CRE age histogram of L-chondrites with low radiogenic gas ages. Alternatively, the low  $^{22}\text{Ne}/^{21}\text{Ne}$  and  $^3\text{He}/^{21}\text{Ne}$  ratios observed in Mifflin might indicate a two-stage exposure history in which the meteoroid was exposed to cosmic rays for at least 30 Ma as an object with a minimum radius of 60 cm, followed by a second-stage exposure of several Ma in an object with a radius of  $\geq 30 \text{ cm}$ .

*Acknowledgments*—Richard Jinkins and his family, and Terry Boudreaux are thanked for donating meteorites for analysis. Other private owners of Mifflin meteorite samples allowed initial inspection and photography. Atul Kumar provided a strewn field map and detailed information of individual masses. Richard Slaughter and others in the Geology Museum and Department of Geoscience, UW-Madison, helped search for and identify the meteorites. Brian Hess, John Fournelle, and Hiromi Konishi are thanked for preparation of Mifflin meteorite sections, and assistance to the electron microprobe analysis, and X-ray diffraction analysis, respectively. We acknowledge Henry Revercomb and Fred Best, Space Science and Engineering Center, UW-Madison, for the permission to use the photo of the fireball (Fig. 1). Mary Diman is thanked for drafting the strewn field map (Fig. 2). We acknowledge careful

reviews by Addi Bischoff, Jutta Zipfel, Greg Herzog, and Associate Editor Alex Ruzicka, which improved the quality of the manuscript, and discussion with Alan Rubin. This work is supported by NASA grants NNX10AH77G (NK), NNX08AY83G (JWV), NNX11AC69G (KN), and NNX09AG39G (AMD), and the Swiss National Science Foundation.

*Editorial Handling*—Dr. Alex Ruzicka

## REFERENCES

- Alexeev V. A. 1998. Parent bodies of L and H chondrites: Times of catastrophic events. *Meteoritics & Planetary Science* 33:145–152.
- Arpesella C. 1996. A low background counting facility at Laboratori Nazionali del Gran Sasso. *Applied Radiation and Isotopes* 47:991–996.
- Bhandari N., Bonino G., Callegari E., Cini Castagnoli G., Mathew K. J., Padia J. T., and Queirazza G. 1989. The Torino, H6, meteorite shower. *Meteoritics* 24:29–34.
- Bhandari N., Murty S. V. S., Shukla P. N., Shukla A. D., Mahajan R. R., Sarin M. M., Srinivasan G., Suthar K. M., Sisodia M. S., Jha S., and Bischoff A. 2002. Itawa Bhopji (L3–5) chondrite regolith breccia: Fall, classification and cosmogenic records. *Meteoritics & Planetary Science* 37:549–563.
- Bischoff A., Rubin A. E., Keil K., and Stöffler D. 1983. Lithification of gas-rich chondrites regolith breccias by grain boundary and localized melting. *Earth and Planetary Science Letters* 66:1–10.
- Bischoff A., Scott E. R. D., Metzler K., and Goodrich C. A. 2006. Nature and origin of meteoritic breccias. In *Meteorites and the early solar system II*, edited by Lauretta D. S. and McSween H. Y. Jr. Tucson, Arizona: University of Arizona Press. pp. 679–712.
- Bischoff A., Horstmann M., Pack A., Laubenstein M., and Haberer S. 2010. Asteroid 2008 TC<sub>3</sub>—Almahata Sitta: A spectacular breccia containing many different ureilitic and chondritic lithologies. *Meteoritics & Planetary Science* 45:1638–1656.
- Bischoff A., Jersek M., Grau T., Mirtic B., Ott U., Kučera J., Horstmann M., Laubenstein M., Herrmann S., Randa Z., Weber M., and Heusser G. 2011. Jesenice—A new meteorite fall from Slovenia. *Meteoritics & Planetary Science* 46:793–804.
- Bogard D. D. 1995. Impact ages of meteorites: A synthesis. *Meteoritics* 30:244–268.
- Bogard D. D., Nyquist L. E., Bansal B. M., Garrison D. H., Wiesmann H., Herzog G. F., Albrecht A. A., Vogt S., and Klein J. 1995. Neutron-capture  $^{36}\text{Cl}$ ,  $^{41}\text{Ca}$ ,  $^{36}\text{Ar}$  and  $^{150}\text{Sm}$  in large chondrites: Evidence for high fluences of thermalized neutrons. *Journal of Geophysical Research* 100:E9401–E9416.
- Brearley A. J. and Jones R. H. 1998. Chondritic meteorite. In *Planetary materials*, edited by Papike J. J. Reviews in Mineralogy, vol. 36. Washington, D.C.: Mineralogical Society of America. pp. 3-1–3-398.
- Clayton R. N., Mayeda T. K., Goswami J. N., and Olsen E. J. 1991. Oxygen isotope studies of ordinary chondrites. *Geochimica et Cosmochimica Acta* 55:2317–2337.
- Dodd R. T. and Jarosewich E. 1979. Incipient melting in and shock classification of L-group chondrites. *Earth and Planetary Science Letters* 44:335–340.

- Evans J. C., Reeves J. H., Rancitelli L. A., and Bogard D. D. 1982. Cosmogenic nuclides in recently fallen meteorites—Evidence for galactic cosmic ray variations during the period 1967–1978. *Journal of Geophysical Research* 87:5577–5591.
- Fries M. D. and Fries J. A. 2010. Doppler weather radar observations of the 14 April 2010 southwest Wisconsin meteorite fall (abstract). *Meteoritics & Planetary Science* 45:A58.
- Garvie L. A. J. 2012. The Meteoritical Bulletin, No. 99. *Meteoritics & Planetary Science* 47:E1–E52.
- Graf T., Baur H., and Signer P. 1990. A model for the production of cosmogenic nuclides in chondrites. *Geochimica et Cosmochimica Acta* 54:2521–2534.
- Heber V. S., Wieler R., Baur H., Olinger C., Friedmann T. A., and Burnett D. A. 2009. Noble gas composition of the solar wind as collected by the Genesis mission. *Geochimica et Cosmochimica Acta* 73:7414–7432.
- Heymann D. 1967. On the origin of hypersthene chondrites: Ages and shock effects of black chondrites. *Icarus* 6:189–221.
- Honda M., Caffee M. W., Miura Y. N., Nagai H., Nagao K., and Nishiizumi K. 2002. Cosmogenic nuclides in the Brenham pallasite. *Meteoritics & Planetary Science* 37:1711–1728.
- Kallemeyn G. W., Rubin A. E., Wang D., and Wasson J. T. 1989. Ordinary chondrites: Bulk compositions, classification, lithophile-element fractionations and composition-petrographic type relationships. *Geochimica et Cosmochimica Acta* 53:2747–2767.
- Korochantseva E. V., Trieloff M., Lorenz C. A., Buykin A. I., Ivanova M. A., Schwarz W. H., Hopp J., and Jessberger E. K. 2007. L-chondrite asteroid breakup tied to Ordovician meteorite shower by multiple isochron  $^{40}\text{Ar}$ - $^{39}\text{Ar}$  dating. *Meteoritics & Planetary Science* 42:113–130.
- Lavielle B., Marti K., Jeannot J.-P., Nishiizumi K., and Caffee M. W. 1999. The  $^{36}\text{Cl}$ - $^{36}\text{Ar}$ - $^{40}\text{K}$ - $^{41}\text{K}$  records and cosmic ray production rates in iron meteorites. *Earth and Planetary Science Letters* 170:93–104.
- Leya I. and Masarik J. 2009. Cosmogenic nuclides in stony meteorites revisited. *Meteoritics & Planetary Science* 44:1061–1086.
- Marti K. 1967. Trapped xenon and the classification of chondrites. *Earth and Planetary Science Letters* 2:193–196.
- Marti K. and Graf T. 1992. Cosmic-ray exposure history of ordinary chondrites. *Annual Review of Earth and Planetary Science* 20:221–243.
- Masarik J., Nishiizumi K., and Reedy R. C. 2001. Production rates of cosmogenic helium-3, neon-21 and neon-22 in ordinary chondrites and the lunar surface. *Meteoritics & Planetary Science* 36:643–650.
- Nakashima D., Nakamura T., and Noguchi T. 2003. Formation history of Cl-like phyllosilicate-rich clasts in the Tsukuba meteorite inferred from mineralogy and noble gas signatures. *Earth and Planetary Science Letters* 212:321–336.
- Nishiizumi K. 2004. Preparation of  $^{26}\text{Al}$  AMS standards. *Nuclear Instruments and Methods in Physics Research Section B* 223–224:388–392.
- Nishiizumi K., Imamura M., Caffee M. W., Southon J. R., Finkel R. C., and McAninch J. 2007. Absolute calibration of  $^{10}\text{Be}$  AMS standards. *Nuclear Instruments and Methods in Physics Research Section B* 258:403–413.
- Rubin A. E. 2002. Post-shock annealing of Miller Range 99301 (LL6): Implications for impact heating of ordinary chondrites. *Geochimica et Cosmochimica Acta* 66:3327–3337.
- Rubin A. E., Rehfeldt A., Peterson E., Keil K., and Jarosewich E. 1983. Fragmental breccias and the collisional evolution of ordinary chondrite parent bodies. *Meteoritics* 18:179–196.
- Schultz L. and Stöffler D. 1993. Shock effects and noble gas concentrations in chondrites (abstract). *Meteoritics & Planetary Science* 28:432.
- Sharma P., Kubik P. W., Fehn U., Gove G. E., Nishiizumi K., and Elmore D. 1990. Development of  $^{36}\text{Cl}$  standards for AMS. *Nuclear Instruments and Methods in Physics Research Section B* 52:410–415.
- Sharma P., Bourgeois M., Elmore D., Granger D., Lipschutz M. E., Ma X., Miller T., Mueller K., Rickey F., Simms P., and Vogt S. 2000. PRIME lab AMS performance, upgrades and research applications. *Nuclear Instruments and Methods in Physics Research Section B* 172:112–123.
- Spergel M. S., Reedy R. C., Lazareth O. W., Levy P. W., and Slate L. A. 1986. Cosmogenic neutron-capture-produced nuclides in stony meteorites. *Journal of Geophysical Research* 91:D483–D494.
- Spicuzza M. J., Day J. M. D., Taylor L. A., and Valley J. W. 2007. Oxygen isotope constraints on the origin and differentiation of the Moon. *Earth and Planetary Science Letters* 253:254–265.
- Stöffler D., Keil K., and Scott E. R. D. 1991. Shock metamorphism of ordinary chondrites. *Geochimica et Cosmochimica Acta* 55:3845–3867.
- Valley J. W., Kitchen N., Kohn M. J., Niendorf C. R., and Spicuzza M. J. 1995. UWG-2, a garnet standard for oxygen isotope ratios: Strategies for high precision and accuracy with laser heating. *Geochimica et Cosmochimica Acta* 59:5223–5231.
- Wasson J. T. and Kallemeyn G. W. 1988. Composition of chondrites. *Philosophical Transactions of the Royal Society of London* A325:535–544.
- Welten K. C., Caffee M. W., Leya I., Masarik J., Nishiizumi K., and Wieler R. 2003. Noble gases and cosmogenic radionuclides in the Gold Basin L4-chondrite shower: Thermal history, exposure history and pre-atmospheric size. *Meteoritics & Planetary Science* 38:157–173.
- Wieler R., Graf T., Pedroni A., Signer P., Pellas P., Fieni C., Suter M., Vogt S., Clayton R. N., and Laul J. C. 1989. Exposure history of the regolithic chondrite Fayetteville: II. Solar-gas-free light inclusions. *Geochimica et Cosmochimica Acta* 53:1449–1459.
- Xie X., Chen M., and Wang D. 2001. Shock-related mineralogical features and P-T history of the Suizhou L6 chondrite. *European Journal of Mineralogy* 13:1177–1190.
- Yeomans D. 2010. Wisconsin fireball caught on tape. JPL news release, April 15, 2010. <http://www.jpl.nasa.gov/news/news.cfm?release=2010-130>.

## SUPPORTING INFORMATION

Additional supporting information may be found in the online version of this article:

**Fig. S1.** Pictures of individual fragments of the Mifflin meteorite that were identified at University of Wisconsin.